Numerical Inverse Interpretation of Single-Hole Pneumatic Tests in Unsaturated Fractured Tuff

by Velimir V. Vesselinov[1,2] and Shlomo P. Neuman[1]

Abstract

A numerical inverse method was used to interpret simultaneously multirate injection and recovery data from single-hole pneumatic tests in unsaturated fractured tuff at the Apache Leap Research Site near Superior, Arizona. Our model represents faithfully the three-dimensional geometry of boreholes at the site, and accounts directly for their storage and conductance properties by treating them as high-permeability and high-porosity cylinders of finite length and radius. It solves the airflow equations in their original nonlinear form and yields information about air permeability, air-filled porosity and dimensionless borehole storage coefficient. Some of this is difficult to accomplish with analytical type-curves. Air permeability values obtained by our inverse method agree well with those obtained by steady-state and type-curve analyses.

Introduction

Recharge often takes place through unsaturated fractured rocks, which are also considered for the possible storage of high-level nuclear waste at Yucca Mountain in Nevada. Yet there are no well-established methods for the hydrogeologic characterization of such rocks. Pneumatic tests offer some important advantages over hydraulic tests in unsaturated fractured rock environments (Guzman and Neuman 1996). Considerable experience with pneumatic tests in fractured rocks has been accumulated at the Apache Leap Research Site (ALRS) near Superior, Arizona (Rasmussen et al. 1990; Guzman et al. 1994, 1996; Guzman and Neuman 1996; Illman et al. 1998; Illman 1999). Similar studies have also been performed at Los Alamos, New Mexico (Cronk 1990), the Yucca Mountain site, Nevada (LeCain 1996, 1998; Wang 1998; Huang 1999) and Box Canyon, Idaho (Benito et al. 1998, 1999). In this paper we describe a numerical inverse method used to interpret simultaneously multirate injection and recovery data from single-hole pneumatic tests in unsaturated fractured tuff at the ALRS. Steady-state analyses of stable pneumatic pressure data from these and many other single-hole tests at the site were conducted earlier by Guzman et al. (1994) and Guzman et al. (1996). Type-curve interpretations of some of the same test data was accomplished by Illman et al. (1998) and Illman and Neuman (2000). Our numerical inverse method is considerably more complex but offers the advantage of solving the airflow equations in their original nonlinear form, representing faithfully the three-dimensional geometry of boreholes at the site, accounting directly for the storage and conductance properties of all open borehole intervals, analyzing pressure data from all phases of a multirate injection and recovery test simultaneously, and being more sensitive to air-filled porosity than are existing type-curve methods.

Not much has been published about the use of numerical inverse methods to interpret pumping or injection tests. Lebbe (1992), Lebbe and de Breuck (1995, 1997), Hvilshøj et al. (1999), Sauer et al. (2000) and Lebbe and van Meir (2000) used such methods to interpret hydraulic tests in saturated aquifer-aquitard systems under assumptions of axisymmetric flow. More important, Lebbe and van Meir (2000) have demonstrated the significance of interpreting multiple tests simultaneously to allow the accurate characterization of medium properties. Cardenas et al. (1999) used a numerical inverse model to analyze pneumatic injection tests at the WIPP site near Carlsbad, New Mexico. Numerical inverse models have also been used successfully for the analysis of various laboratory tests by Finsterle and Pruess (1995), Finsterle and Persoff (1997), Finsterle and Faybishenko (1999), and others.

Single-Hole Pneumatic Tests at the ALRS

The Apache Leap Research Site (ALRS) is near Superior in central Arizona. The site includes 16 vertical and slanted (at about 45°) boreholes (Figure 1). All boreholes are open, except for the upper 1.8 m of each borehole, which is cased. The surface exposure of the boreholes was covered with a thick plastic sheet to minimize infiltration and evaporation.

Guzman et al. (1994, 1996) and Guzman and Neuman (1996) conducted single-hole pneumatic injection tests at the site over borehole intervals of various lengths. This paper concerns some of the 184 tests they have conducted in six boreholes (X2, Y2, Y3, Z2, V2, and W2A) by setting the packers 1 m apart (Figure 1). The packers were 3 m long. During each test, the borehole interval above the top packer and all surrounding boreholes were open to the atmosphere. The tests were conducted by maintaining a constant injection rate until air pressure became relatively stable and remained so for some time. The injection rate was then incremented by a constant value and the procedure repeated. Two or more such incremental steps were performed in each borehole segment while recording the air injection rate, pressure, temperature and relative humidity during injection and, in most cases, recovery. The injection flow rate varied from 9.8×10^{-8} to 4.4×10^{-4} kg/s (from 0.0049 to 22.0 L/min under standard conditions) and the steady-state pressure buildup in the injection interval ranged from 0.49 to 273 kPa. The time required for pressure in the injection interval to stabilize typically ranged from 30 to 60 minutes, increased with flow rate, and might have at times exceeded 24 hours.

[1]Department of Hydrology and Water Resources, University of Arizona, Tucson, AZ 85721-0011

[2]Now at Hydrology, Geochemistry and Geology Group, Los Alamos National Laboratory, Los Alamos, NM 87545

Received June 2000, accepted March 2001.

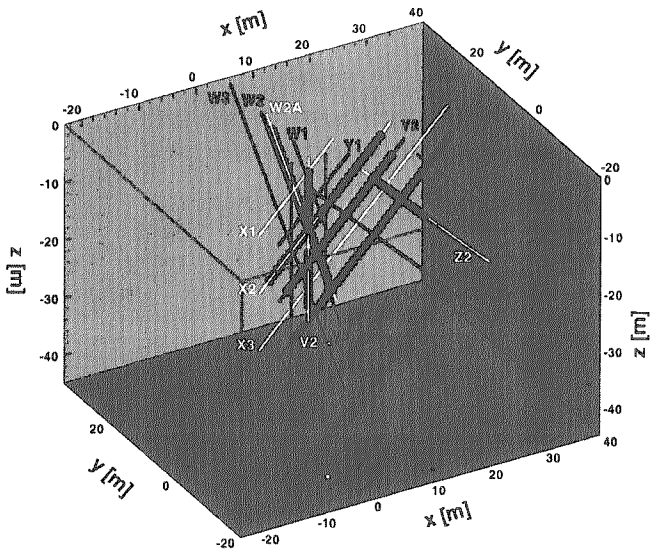

Figure 1. Three-dimensional perspective of boreholes at the site and center locations (black circles) of 1 m single-hole test intervals employed by Guzman et al. (1996). The gray box defines the computational domain.

Conceptual Model of Airflow

The conceptual model of airflow during pneumatic tests at the site was originally formulated by Guzman and Neuman (1996) and Guzman et al. (1996). It is consistent with pneumatic-test interpretations by Illman et al. (1998), Illman (1999), and Illman and Neuman (2000). According to this model, the high capillary retention properties of the porous matrix causes water to be drawn from fractures into the matrix, leaving the fractures filled primarily with air, and making it difficult for air to flow through the matrix. Therefore, airflow during pneumatic tests occurs primarily through fractures, most of which contain little water. As the matrix is virtually saturated with water, air storage in the matrix is not expected to impact the results of pneumatic tests. While two-phase flow of air and water is taking place in the fractures and the matrix, it appears appropriate to disregard the movement of water in fractures and air in the matrix, by considering only single-phase airflow in the fractures. In fact, the air entry pressure of matrix is estimated to range from 15.6 to 98 kPa (Vesselinov 2000). It compares with air pressures applied to injection intervals during single-hole pneumatic tests at the ALRS, which, however, die rapidly with distance from these intervals. Therefore, one can expect two-phase flow effects to be important at most in the close vicinity of the injection interval.

Inertial effects were observed by Guzman and Neuman (1996) in only a few single-hole test intervals intersected by widely open fractures. Enhanced permeability due to slip flow (the Klinkenberg effect) also appeared to be of little relevance to the interpretation of pneumatic tests at the ALRS (Guzman and Neuman 1996; Illman et al. 1998). The fracture data collected at the ALRS suggest that the fractures form a dense interconnected three-dimensional network (Vesselinov 2000). It is therefore reasonable to represent the fractured rock at the site as a single equivalent continuum. For purposes of single-hole test interpretation, we treat this continuum as if it was uniform and isotropic. We additionally assume that airflow at the ALRS takes place under isothermal conditions, ignoring adiabatic effects and differences in temperatures between injected and ambient air in the rock.

Methodology

Governing Equations

Airflow in porous continua is governed by (Bear 1972):

$$\nabla \cdot \left(\frac{k\rho}{\mu} \nabla p \right) + \frac{\partial}{\partial z} \left(\frac{kg\rho^2}{\mu} \right) + q_w = \phi \frac{\partial \rho}{\partial t} \tag{1}$$

subject to initial and generalized boundary conditions

$$p = p_0 \text{ on } \Omega \text{ at } t = 0 \tag{2}$$

$$\left(\frac{k\rho}{\mu} \nabla p \right) \cdot n = \upsilon (p_f - p) + q_b \text{ along } \Gamma \tag{3}$$

where p is absolute air pressure (M/LT^2), ρ is air density (M/L^3), μ is air dynamic viscosity (M/LT), k is air permeability (L^2), ϕ is air-filled porosity (–), q_w is a source term (M/L^3T), Ω is the flow domain, Γ is its boundary, n is a unit vector normal to Γ, p_f is prescribed air pressure (M/LT^2) on the boundary Γ, q_b is prescribed air mass flux (M/L^2T) normal to the boundary Γ, υ (T/L) is a parameter controlling the type of boundary conditions (first or second type if $\upsilon = 0$ or $\upsilon \to$ to ∞, respectively; third type otherwise) and g is acceleration due to gravity (L/T^2; 9.8 m/s^2). The absolute air pressure p (N/m^2) and air density ρ (kg/m^3) are related through the equation of state

$$\rho = \frac{pM}{ZRT} \tag{4}$$

where Z is a dimensionless compressibility factor depending on air pressure and temperature, M is molecular mass (kg), T is absolute temperature (^{0}K), and R is the universal gas constant (8.314 J/[^{0}K · mol]). Under isothermal conditions, T is constant and nonlinearity is due solely to dependence of ρ and μ on p. Within the range of pressures and temperatures encountered during pneumatic test at the ALRS, the dimensionless compressibility factor, Z, is approximately constant and equal to 1.

The mass flow rate Q_w (M/T) from the injection interval into the rock (proportional to q_w in Equation 1) satisfies the mass-balance equation

$$Q_{inj} - Q_w = \frac{dM}{dt} \tag{5}$$

where Q_{inj} (M/T) is the rate at which air mass is injected into the packed-off interval and M is the air mass within this interval. The right side of Equation 5 can be rewritten as

$$\frac{dM}{dt} = \frac{dM}{dp_w} \frac{dp_w}{dt} = V_w \frac{d\rho}{dp_w} \frac{dp_w}{dt} \tag{6}$$

where p_w is air pressure in the injection interval and V_w (L^3) is its nominal volume. Considering that air compressibility, C_a (LT^2/M), is defined as

$$C_a = \frac{1}{\rho} \frac{d\rho}{dp} \tag{7}$$

one can rewrite Equation 5 as

$$Q_{inj} - Q_w = V_w \rho C_a \frac{dp_w}{dt} \quad (8)$$

Since the dimensionless compressibility factor, Z, in Equation 4 is approximately constant, $C_a \approx 1/p_w$. Assuming that the pressures of injected air are equal to that within the injection interval, the corresponding air densities are also equal (as T is taken to be constant). One can therefore recast Equation 8 in volumetric form as

$$Q'_{inj} - Q'_w = V_w C_a \frac{dp_w}{dt} \approx V_w \frac{1}{p_w} \frac{dp_w}{dt} \quad (9)$$

where $Q' = Q/\rho$, (L^3/T). Here the right side represents the volumetric rate of change in storage within the injection interval. The storage depends on air compressibility and decreases with an increase in absolute air pressure within the injection interval. During air injection, the associated storage effect decreases with time as air pressure in the injection interval stabilizes. During pressure recovery, $Q'_{inj} = 0$ and theoretically there is no borehole storage effect.

In the absence of flow from the packed-off interval into the rock, $Q'_w = 0$ and Equation 9 yields

$$\Delta\tilde{p} = \exp(\tilde{t}) - 1 \quad (10)$$

where $\Delta\tilde{p} = \frac{p - p_0}{p_0}$ is dimensionless pressure buildup and $\tilde{t} = t \frac{Q'_{inj}}{V_w}$ is dimensionless time. Hence when pneumatic pressure is plotted versus time on log-log paper, borehole storage manifests itself as an exponential curve at early time. Only when pressure buildup is small ($\Delta\tilde{p} \approx 1$) does $\tilde{t}$ come close to 1 and Equation 10 yields, to a first-order of approximation,

$$\Delta\tilde{p} \approx \tilde{t} \quad (11)$$

The latter results in a straight line with unit gradient on log-log paper, which characterizes borehole storage in the constant compressibility case.

For three-dimensional airflow from a point source, it is convenient to define a dimensionless borehole storage coefficient, C_D, as (Illman et al. 1998)

$$C_D = \frac{C_w p}{3 V_w \phi} \quad (12)$$

where $C_w = V_S C_a$ (L^4T^2/M) is a storage coefficient characterizing the injection interval and V_S (L^3) is the effective storage volume of this interval. Since V_S is equal to $V_w \phi_w$ where ϕ_w (–) is an effective porosity of the interval, the above can be also written as

$$C_D = \frac{V_S}{3 V_w \phi} = \frac{\phi_w}{3\phi} \quad (13)$$

The effective porosity ϕ_w can be larger than 1 to accommodate effective interval volumes that are larger than their nominal volume V_w. In this way, ϕ_w may account for air storage not only in the injection interval proper, but also in large openings within the surrounding rock.

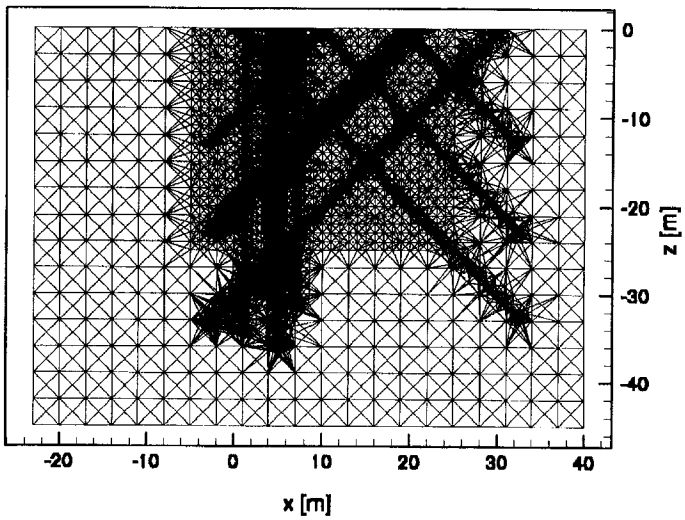

Figure 2. Side view of computational grid perpendicular to the x-z plane.

Numerical Inverse Model

A single numerical inverse model was developed for the analysis of both single-hole and cross-hole pneumatic tests at the ALRS (Vesselinov 2000). This model is therefore more complex than would have been required for the interpretation of single-hole tests alone. The model simulates airflow by means of a three-dimensional finite-element/finite-volume code, FEHM version 96-05-07, developed at Los Alamos National Laboratory, New Mexico (Zyvoloski et al. 1988, 1996, 1997). Our decision to use FEHM was based in part on the ability of this code to simulate nonisothermal two-phase flow of air and water in dual porosity and/or dual permeability continua, and to account for discrete fractures, should the need to do so arise (it never did). Variations in air viscosity are ignored in FEHM, which is justified for the ranges of pressures and temperatures recorded during pneumatic tests at the ALRS. Air dynamic viscosity μ is set equal to 1.82×10^{-8} Pa · s, which is appropriate for the test conditions. Since we treated the rock as isotropic, we used the finite-volume (integrated finite-difference) option, which is computationally more efficient than finite elements. Under this option, each node is associated with a volume defined by three-dimensional Voronoï diagrams based on Delaunay tessellation on a grid of tetrahedral elements (Trease et al. 1996). Model parameters such as k and ϕ are defined at nodes rather than over elements, and are representative of the corresponding control volumes. The code uses the algorithm GZSOLVE (Zyvoloski and Robinson 1995) to provide a robust implementation of the Newton-Raphson method for sparse systems of nonlinear equations.

The three-dimensional computational domain measured 63 m in the x direction, 54 m in the y direction and 45 m in the z direction (Figure 1). The side and bottom boundaries of the flow domain were impermeable to airflow. These boundaries were placed sufficiently far from the tested intervals to have virtually no effect on simulated pneumatic tests. The top boundary coincided with the ground surface and was maintained at a constant and uniform barometric pressure of 100 kPa. Initial air pressure, p_0, was set equal to the same pressure throughout the flow domain.

Due to the high compressibility of air, we expected borehole storage to have a measurable impact on pneumatic test responses. Our numerical model was therefore designed to represent the actual geometry of boreholes at the site, and to account directly for conductive and storage effects in all open borehole intervals by treating them as high-

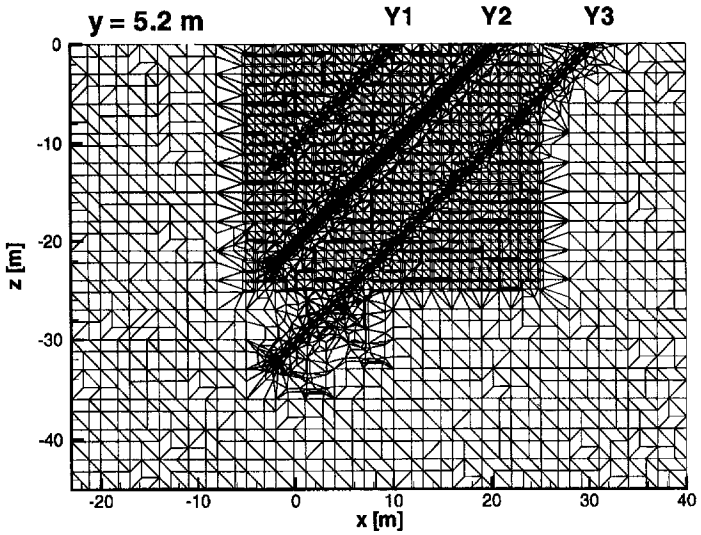

Figure 3. Vertical cross section through computational grid along injection borehole Y2.

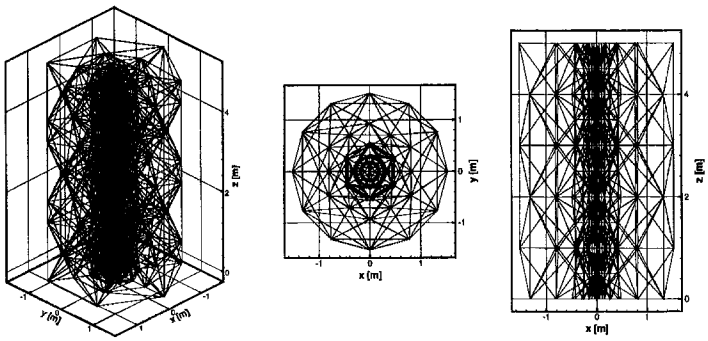

Figure 4. Three-dimensional representation of computational grid along injection borehole.

permeability and high-porosity cylinders of finite length and radius.

The grid generator X3D (Cherry et al. 1996; Trease et al. 1996) was adopted to automatically subdivide the computational domain into tetrahedral elements. Grids were created automatically in a manner that enhances the computational efficiency of the FEHM simulator. The grid employed to simulate injection in borehole Y2 is illustrated by means of two-dimensional images in Figures 2 and 3. It contains 39,264 nodes and 228,035 elements. Figure 2 shows a view of the grid perpendicular to the x-z plane along which borehole Y2 is located. Dark areas correspond to fine discretization in the vicinity of boreholes. Figure 3 shows a cross-sectional view of the grid along a vertical plane that contains the injection borehole Y2. A 5 m long segment of the three-dimensional computational grid along this borehole is shown in Figure 4. The grid is designed so that the sum of computational volumes associated with nodes along the borehole is close to the actual volume of the borehole.

To simulate the effect of open borehole intervals on pressure propagation, these intervals were treated as highly permeable and highly porous media of cylindrical shape. The permeability and effective porosity of nodes along these intervals were set to 3.23×10^{-4} m^2 and 1.0 m^3/m^3, respectively. In some cases, the latter would be automatically adjusted by the inverse model. Nodes along packers were assigned zero permeability and a low porosity of 10^{-5} m^3/m^3 for the respective nodes. In some cases, we selectively "eliminated" boreholes by setting the permeabilities and porosities of nodes along them equal to those of the surrounding rock.

The net result was a complex three-dimensional grid that accurately represents the geometry, flow properties, and storage capabilities of vertical and inclined boreholes at the ALRS; is able to represent, with a high degree of resolution, steep gradients around the injection interval, as well as pressure interference between boreholes, no matter how closely spaced; and assures smooth transition between fine borehole grids having radial structures and surrounding coarser grids having regular structures.

To interpret single-hole test data, we employed the parameter estimation and optimization code (PEST) (Doherty et al. 1994). We developed a series of pre- and postprocessing codes to allow automatic communication between FEHM and PEST. PEST uses a variant of the Levenberg-Marquardt algorithm to estimate a vector a of the unknown parameters by minimizing a weighted square difference

$$\Phi(\mathbf{a}) = \sum_{i=1}^{N} w_i [p_i(\mathbf{a}) - p_i^*]^2 \qquad (14)$$

between simulated and observed air pressures, $\mathbf{p}(\mathbf{a})$ and $\mathbf{p}^*$, respectively. Here N is the number of measurements in time t, and w_i is the relative weight of each measurement in the optimization process. In the most general case, the M-dimensional vector **a** includes k and ϕ (permeability and porosity of the rock), and ϕ_w (effective porosity of the injection interval). Following optimization, PEST computes the covariance matrix of the estimated parameters provided the corresponding normal matrix is nonsingular (Doherty et al. 1994; Vesselinov 2000). PEST also calculates the corresponding correlation matrix and performs an eigenanalysis on the covariance matrix. Since the covariance matrix is positive definite, eigenvalues are real and eigenvectors are mutually orthogonal, representing the axes of an M-dimensional probability ellipsoid. PEST then defines the separate 95% confidence intervals for the estimates. The error analysis assumes that the measurements are mutually uncorrelated and the model is linear. For the confidence intervals, it is also assumed that the estimation errors are Gaussian. In our case, none of these assumptions are expected to be fulfilled and, therefore, we consider the corresponding statistics merely as crude approximations.

Enhanced computational efficiency of the Levenberg-Marquardt algorithm can be achieved by parallelizing the evaluation of the sensitivity (Jacobian) matrix (Doherty et al. 1994; Vesselinov 2000). Doherty (1997) created a parallel UNIX version of PEST. We have modified this parallel version so as to better use the computational resources of a standard UNIX multiprocessor environment. We have further altered PEST to allow efficient restarting of the optimization process, if and when it terminates prematurely, so as to virtually eliminate loss of computational time. The parallelized version of the inverse model was run on the University of Arizona SGI Origin 2000 multiprocessor supercomputer, which had operated at a speed of 300 MHz. On average, each analysis required about 50 forward simulations of the single-hole tests by means of FEHM, and took about four hours of effective computational time.

Results and Discussion

We consider here four single-hole pneumatic tests conducted in borehole Y2, details of which are listed in Tables 1 and 2. Borehole Y2 is slanted and located more or less in the center of the tested rock volume (Figure 1). For each test, we present a separate analysis of pressure data from the first injection step of the test (labeled A) and of data from the entire test, including multiple

Table 1
Single-Hole Pneumatic Tests Analyzed by Inverse Modeling (Guzman et al. 1996)

Test	Length of Injection Interval [m]	Distance from top of Y2 to Center of Injection Interval [m]
JG0921	2.0	16.10
JGC0609	1.0	13.85
JHB0612	1.0	15.81
JJA0616	1.0	17.77

Table 2
Single-Hole Test Data Analyzed by Inverse Modeling (Guzman et al. 1996)

Test	Injection Step	Duration [min]	Injection Rate [cm^3/min]	Injection Rate [kg/s]
JG0921	A	66.0	400.7	8.014×10^{-6}
	B	63.05	1983.6	3.967×10^{-5}
	R	11.12	0.0	0.0
JGC0609	A	144.9	499.2	9.984×10^{-6}
	B	161.1	999.8	2.000×10^{-5}
	C	220.9	1501.0	3.002×10^{-5}
	D	195.1	1801.2	3.602×10^{-5}
	R	286.0	0.0	0.0
JHB0612	A	109.65	502.3	1.005×10^{-5}
	B	100.05	1201.1	2.402×10^{-5}
	C	95.25	1951.7	3.903×10^{-5}
	R	62.05	0.0	0.0
JJA0616	A	91.9	300.3	6.001×10^{-6}
	B	132.1	800.8	1.602×10^{-5}
	C	100.0	1301.0	2.602×10^{-5}
	R	726.0	0.0	0.0

injection steps (labeled A, B, C, D) and recovery (labeled R). Our analyses of the first step consider three cases: no open borehole intervals, an open injection interval, and open intervals in all boreholes. In the first case, we ignore open borehole effects; permeability and porosity are uniform over the entire computational grid (including nodes along boreholes). In the second case, we consider the effect of an open injection interval by assigning to it high permeability and high porosity values. In the last case, the effects of all open borehole intervals are considered by treating them as high-permeability and high-porosity cylinders.

To analyze the single-hole tests numerically, a set of match points is defined for each injection step and recovery. The match points are distributed more or less evenly along a log-transformed time axis. On the average, there are 10 match points per injection step. These are assigned unit weights w_i when analyzing pressure data from the first step of a test. When analyzing pressure data from all steps simultaneously, the weights wi are made inversely proportional to the observed pressure values p_i^*. Doing the latter is analogous to defining the objective function as the weighted sum of squared differences between the logarithms of simulated pressures p_i and observed measurements p_i^* (Doherty et al. 1994). This allows better representation of weak pressure responses that characterize early-time pressure buildup and recovery. Our numerical inverse results are compared against those obtained by steady-state (Guzman et al. 1996) and p^2-based transient type-curve (Illman et al. 1998; Illman and Neuman 2000) analyses.

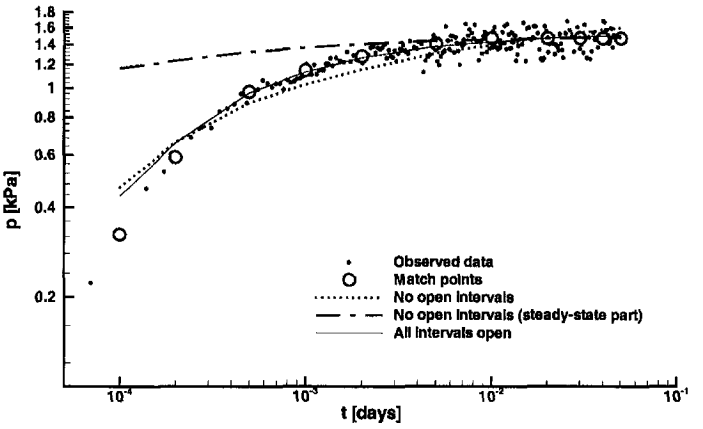

Figure 5. Pressure data from the first injection step during test JG0921 interpreted by various inverse models.

Test JG0921

Parameters estimated for test JG0921 by both analytical and numerical approaches are summarized in Table 3. In the table, and through the rest of the text, the ± range represents separate 95% confidence intervals identified by our numerical inverse model. Both steady-state (Guzman et al. 1996) and transient (Illman et al. 1998) analytical interpretations of the first injection step data gave similar estimates of k; neither of the two analyses would yield ϕ or C_D estimates. The type-curve interpretation did not produce a satisfactory match between analytical and measured pressure responses (Illman et al. 1998).

The matches between pressure values computed by the numerical inverse model, and measured during the first injection step of the test, are depicted in Figure 5. When open borehole intervals (including that used for injection) are not considered in the simulation, our numerical inverse model yields a match that is not entirely satisfactory. The estimate of k is close to that obtained by analytical methods, but the estimate of ϕ appears to be too high for fractures (Table 3). When only steady-state pressure data are included in the inverse analysis, the match at early time is poor, but the analysis yields a k value equivalent to that obtained by the steady-state method. Here the estimate of ϕ is based entirely on the time at which a steady-state regime commences, which we have implicitly specified through the first match point representing the steady-state portion of the pressure record ($t \approx 0.008$ days). The model is therefore quite insensitive to ϕ and fails to yield a finite confidence interval for either parameter as the normal matrix becomes singular. When the effect of all open borehole intervals is included in the analysis, and the effective porosity of the injection interval, ϕ_w, is allowed to vary simultaneously with k and ϕ, the match improves significantly.

The large confidence interval associated with ϕ (of the same order as its estimate; Table 3) shows low sensitivity to this parameter and indicates that its estimate is uncertain. Eigenvalues and eigenvectors of the covariance matrix of the parameter estimates are listed in Table 4. The first eigenvector is dominated entirely by k, indicating that this parameter is very well defined. The second and third eigenvectors show correlation between ϕ and ϕ_w, rendering both estimates less certain. It reflects the fact that the transient test data are influenced by borehole storage.

As previously discussed, an increase in absolute air pressure within the injection interval reduces its storage capacity. Figure 6 depicts changes in storage during injection steps and recovery (measured relative to those established at the beginning of the

Table 3
Parameter Estimates for Test JG0921

Type of Analysis	k [m^2]	ϕ [m^3/m^3]	ϕ_w [m^3/m^3]	C_D [–]
Analytical steady-state (A)	2.8×10^{-14}			
Analytical transient				
• Spherical flow (A)	2.6×10^{-14}			
Inverse modeling				
• No open intervals (A)	$2.3 \times 10^{-14} \pm 2.6 \times 10^{-16}$	$4.5 \times 10^{-1} \pm 1.9 \times 10^{-3}$		
• No open intervals (A; steady-state)	2.8×10^{-14}	4.6×10^{-3}		
• All intervals open (A)	$2.2 \times 10^{-14} \pm 4.4 \times 10^{-16}$	$6.7 \times 10^{-3} \pm 4.7 \times 10^{-3}$	$7.0 \times 10^{-1} \pm 6.7 \times 10^{-3}$	3.5×10^{1}
• All intervals open (A,B,R)	$2.4 \times 10^{-14} \pm 7.1 \times 10^{-16}$	$1.4 \times 10^{-2} \pm 1.7 \times 10^{-3}$	$8.0 \times 10^{-1} \pm 4.6 \times 10^{-2}$	1.9×10^{1}

Table 4
Eigenanalysis of Covariance Matrix of Estimation Errors Obtained from Interpretation of First Step During Test JG0921

Parameters	Eigenvectors		
k [m^2]	1.000	5.4264×10^{-14}	-3.5632×10^{-14}
ϕ [m^3/m^3]	3.0424×10^{-14}	–0.8766	–0.4812
ϕ_w [m^3/m^3]	5.7346×10^{-14}	–0.4812	0.8766
Eigenvalues	1.5993×10^{-32}	2.2001×10^{-6}	1.0564×10^{-5}

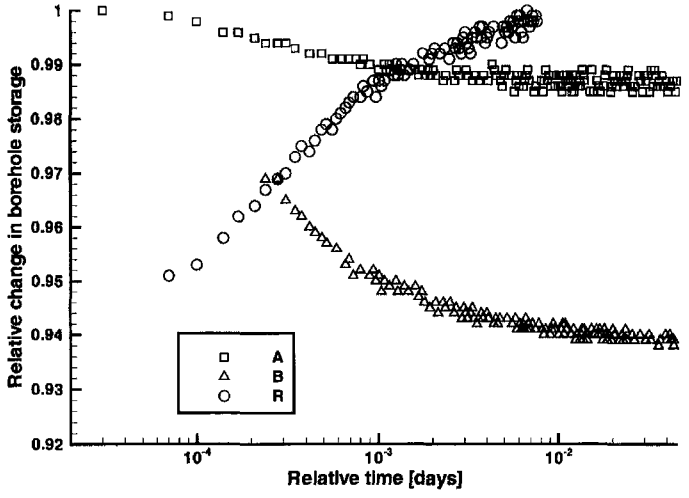

Figure 6. Relative change in borehole storage versus relative time corresponding to injection steps and recovery during test JG0921.

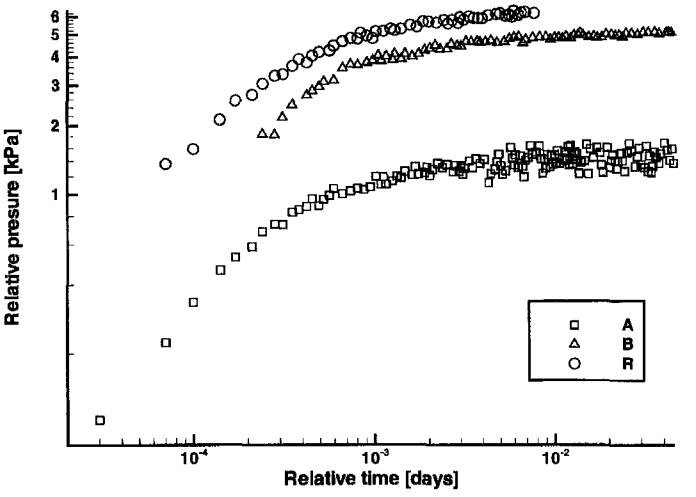

Figure 7. Relative pressure versus relative time corresponding to injection steps and recovery during test JG0921.

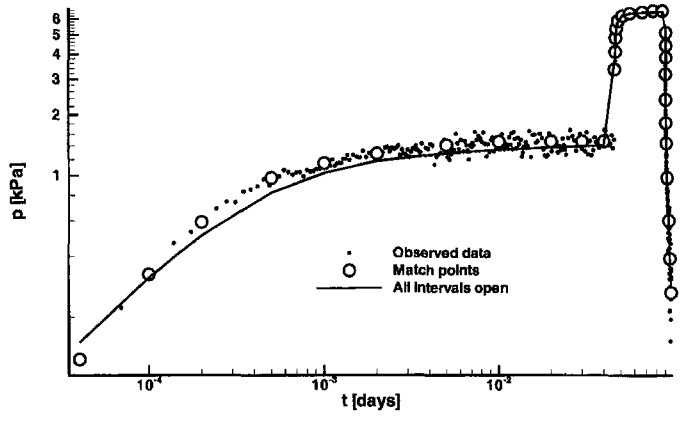

Figure 8. Pressure data from first injection steps and recovery during test JG0921 interpreted by inverse model.

test) due to changes in air compressibility, C_a, plotted versus time measured relative to the end of the preceding step. Since relative pressure buildups during the injection steps were not significant in comparison to the initial air pressure (p_0 = 100 kPa), changes in borehole storage were not substantial. However, the effect of air compressibility on borehole storage appears to be a factor in our ability to obtain a good match between numerically simulated and observed pressures during the first injection step, in contrast to the analytical type-curve method (Illman et al. 1998), which was unable to achieve such a match in this particular case.

Figure 7 depicts relative pressure during each step and recovery plotted versus relative time. We see a very distinct unit slope during the first step (labeled A) of the test. To the extent that storage impacts the other two pressure records in the figure, this effect is not clearly discernible. Storage in the injection interval has theoretically no effect on recovery data, which should therefore be ideal for the estimation of ϕ and ϕ_w (respectively C_D). We, thus, expect a simultaneous analysis of pressure data from the entire test to yield a more reliable estimate of parameters than is possible based only on data from the first step.

A reasonably good fit of our model (accounting for all open borehole intervals) to the entire two-step pressure buildup and recovery record is shown in Figure 8. The corresponding parameter estimates are listed in Table 3. Table 5 shows that each eigenvector of the cor-

Table 5
Eigenanalysis of Covariance Matrix of Estimation Errors Obtained from Interpretation of All Injection Steps and Recovery During Test JG0921

Parameters	Eigenvectors		
k [m^2]	1.000	-2.3433×10^{-13}	1.3300×10^{-15}
ϕ [m^3/m^3]	-2.3431×10^{-13}	-1.000	-6.1345×10^{-3}
ϕ_w [m^3/m^3]	-2.7675×10^{-15}	-6.1345×10^{-3}	1.000
Eigenvalues	8.2641×10^{-32}	6.6215×10^{-7}	5.1651×10^{-4}

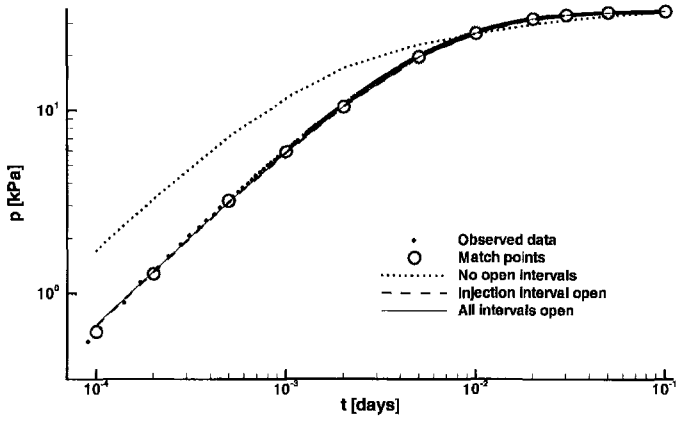

Figure 9. Pressure data from first injection step during test JGC0609 interpreted by various inverse models.

responding estimation covariance matrix is now dominated almost entirely by one parameter, showing lack of correlation between the estimates and suggesting that they are of a high quality.

Test JGC0609

Results of analyzing pressure data from test JGC0609 by various methods are listed in Table 6. Steady-state (Guzman et al. 1996) and type-curve (spherical flow model) (Illman et al. 1998) analyses gave close values for k. As in the previous test, the type-curves did not match well the entire pressure record (Illman et al. 1998).

Numerical inverse results are compared with measured values in Figure 9. In the absence of open borehole intervals, the inverse model yields a poor fit; upon including the injection interval, the fit improves dramatically; incorporating the storage capacity of all open boreholes results in an equally good fit. The last two matches yield similar estimates of parameters (Table 3). As we have discussed in the methodology section (Equations 12 and 13), ϕ_w is allowed to take on values in excess of 1, as a way of accounting for an effective borehole volume that is larger than the one originally built into the computational grid. Therefore, $\phi_w > 1$ is plausible, implying that the effective storage volume of the injection interval, V_S, exceeds its nominal volume, V_w. The excess is most probably due to large openings in the surrounding rock, which are pneumatically well-connected with the injection interval. However, the available single-hole test data do not allow us to distinguish unambiguously between the roles that the borehole and the surrounding rock (fractures and matrix) may play in controlling the observed storage effect. Despite the good fit, the estimates of ϕ do not seem reliable because of the relatively large confidence intervals. For the last match, the eigenanalysis results displayed in Table 7 indicate that there is a correlation between ϕ and ϕ_w, most probably due to the influence of storage during the transient period of the test.

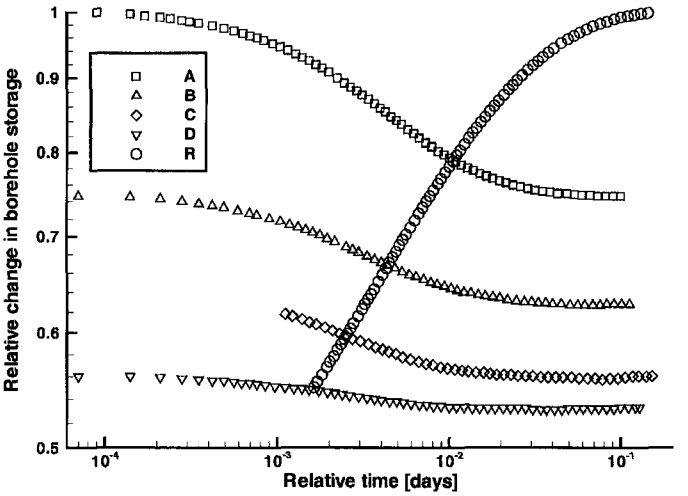

Figure 10. Relative change in borehole storage versus relative time corresponding to injection steps and recovery during test JGC0609.

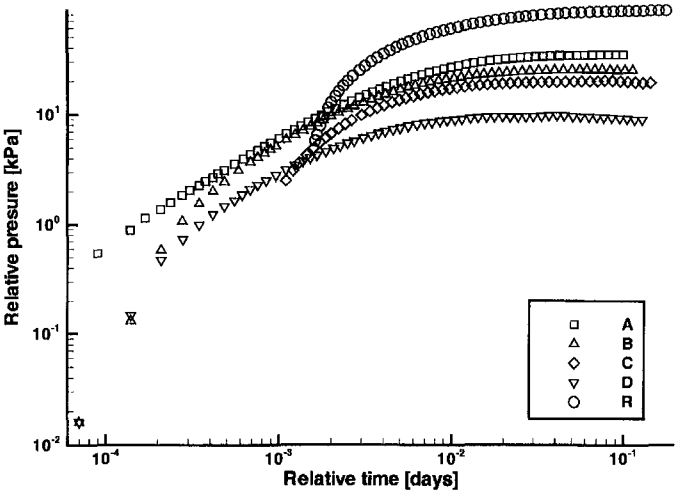

Figure 11. Relative pressure versus relative time corresponding to injection steps and recovery during test JGC0609.

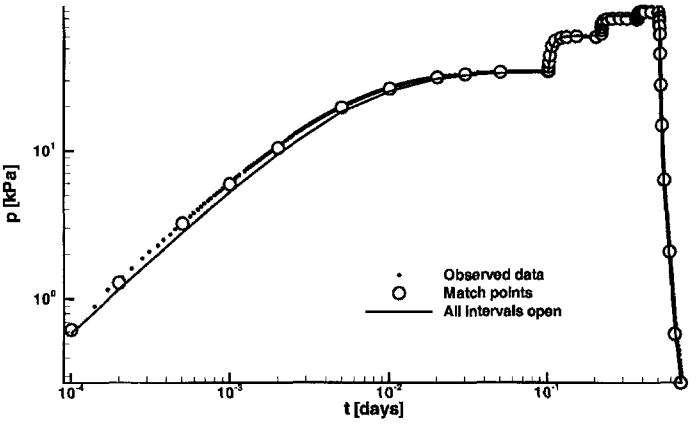

Figure 12. Pressure data from all injection steps and recovery during test JGC0609 interpreted by inverse model.

Figure 10 shows changes in borehole storage due to changes in C_a versus relative time. Pressure buildups are now comparable to the initial air pressure (100 kPa) and, therefore, changes in borehole storage are substantial even during the first injection step (except for very early time). This may explain why type-curve matches (Illman et al. 1998) were not entirely satisfactory in this case.

Figure 11 depicts relative pressure versus relative time for the four injection steps (labeled A through D, respectively) and

Table 6
Parameter Estimates for Test JGC0609

Type of Analysis	k [m^2]	ϕ [m^3/m^3]	ϕ_w [m^3/m^3]	C_D [–]
Analytical steady-state (A)	2.0×10^{-15}			
Analytical transient				
• Spherical flow (A)	2.9×10^{-15}			
Inverse modeling				
• No open intervals (A)	$1.8 \times 10^{-15} \pm 3.9 \times 10^{-15}$	$5.0 \times 10^{-1} \pm 4.2 \times 10^{-2}$		
• Open injection interval (A)	$1.6 \times 10^{-15} \pm 2.6 \times 10^{-17}$	$4.8 \times 10^{-3} \pm 9.4 \times 10^{-3}$	$1.3 \pm 2.6 \times 10^{-2}$	9.0×10^{1}
• All intervals open (A)	$1.6 \times 10^{-15} \pm 1.3 \times 10^{-17}$	$5.5 \times 10^{-3} \pm 4.7 \times 10^{-3}$	$1.3 \pm 1.7 \times 10^{-2}$	7.9×10^{1}
• All intervals open (A,B,C,R)	$1.7 \times 10^{-15} \pm 4.1 \times 10^{-17}$	$3.6 \times 10^{-3} \pm 2.8 \times 10^{-4}$	$1.5 \pm 6.3 \times 10^{-2}$	1.4×10^{2}

Table 7
Eigenanalysis of Covariance Matrix of Estimation Errors Obtained from Interpretation of First Step During Test JGC0609

Parameters	Eigenvectors		
k [m^2]	1.000	2.943×10^{-15}	4.9941×10^{-16}
ϕ [m^3/m^3]	2.9627×10^{-15}	–0.9758	–0.2188
ϕ_w [m^3/m^3]	1.5247×10^{-16}	–0.2188	0.9758
Eigenvalues	3.0691×10^{-36}	1.7338×10^{-6}	6.7666×10^{-5}

Table 8
Eigenanalysis of Covariance Matrix of Estimation Errors Obtained from Interpretation of All Injection Steps and Recovery During Test JGC0609

Parameters	Eigenvectors		
k [m^2]	1.000	-1.1142×10^{-13}	1.3489×10^{-16}
ϕ [m^3/m^3]	-1.1142×10^{-13}	–1.000	-4.8913×10^{-4}
ϕ_w [m^3/m^3]	-1.8939×10^{-16}	-4.8913×10^{-14}	1.000
Eigenvalues	1.6206×10^{-34}	1.8990×10^{-8}	9.7135×10^{-4}

recovery (labeled R). Here again we see that only data corresponding to step A exhibit an unambiguous one-to-one slope at early time, while all other data appear to be less influenced by storage. The one-to-one slope also demonstrates that there is no significant change in borehole storage due to air compressibility at early time. We therefore expect a simultaneous analysis of pressure data from the entire test to yield a more reliable estimate of parameters, especially ϕ, than is possible based only on data from the first step.

A fit of our model to the entire pressure record, including recovery data, yields a good match (Figure 12). The model appears sensitive to all three parameters (Table 8) whose estimates seem reasonable (Table 6).

Test JHB0612

Table 9 lists parameters obtained by various methods of analysis from pressure data recorded during test JHB0612. Transient type-curve analysis using a spherical flow model (Illman et al. 1998; Illman and Neuman 2000) identified a k close to that obtained by steady-state analysis (Guzman et al. 1996). The type-curves for a radial flow model

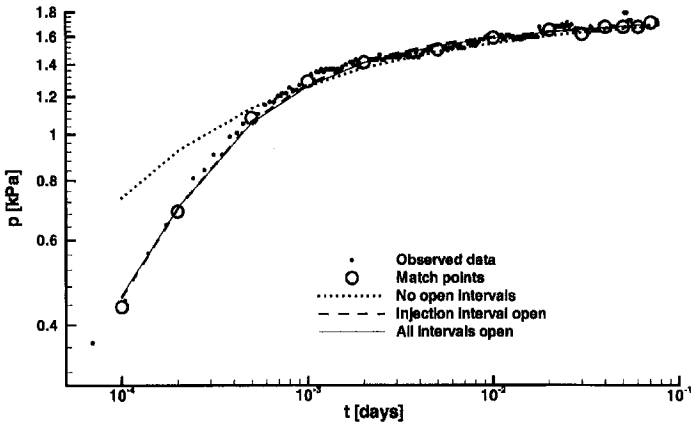

Figure 13. Pressure data from first injection step during test JHB0612 interpreted by various inverse models.

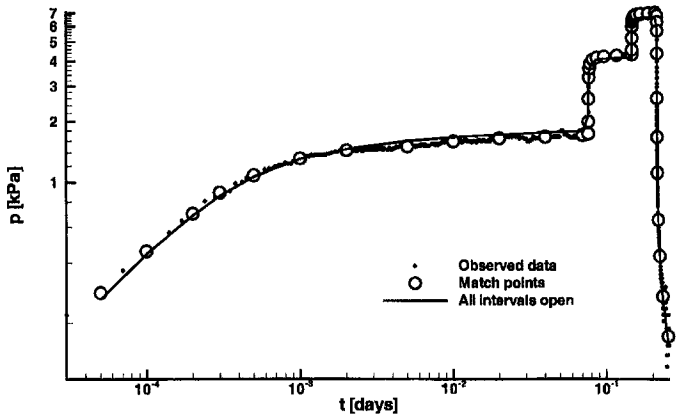

Figure 14. Pressure data from all injection steps and recovery during test JHB0612 interpreted by inverse model.

(Illman et al. 1998) yielded a k that is an order of magnitude lower than the steady-state value, and ϕ, which is much too low for the tested rock. Neither of these two sets of type-curves matched the observed pressures record (Illman et al. 1998): the spherical model failed at late time, the radial model at early time. Illman et al. (1998) also considered type-curves corresponding to a single horizontal or vertical fracture that intersects the injection interval; these models also failed to match the pressure record. Figure 13 indicates that inverse analysis yields a good fit (when incorporating the injection interval), but the model is insensitive to ϕ and ϕ_w estimates (Table 9). These estimates therefore remain uncertain. As in test JG0921, pressure buildups are small compared to

Table 9
Parameter Estimates for Test JHB0612

Type of Analysis	k [m^2]	ϕ [m^3/m^3]	ϕ_w [m^3/m^3]	C_D [–]
Analytical steady-state (A)	4.8×10^{-14}			
Analytical transient				
• Spherical flow (A)	6.5×10^{-14}			
• Radial flow (A)	1.3×10^{-13}	4.0×10^{-5}		1.0×10^{4}
Inverse modeling				
• No open intervals (A)	$5.2 \times 10^{-14} \pm 1.1 \times 10^{-16}$	$5.0 \times 10^{-1} \pm 1.2 \times 10^{-3}$		
• Open injection interval (A)	$4.0 \times 10^{-14} \pm 4.4 \times 10^{-16}$	$8.1 \times 10^{-2} \pm 1.6 \times 10^{6}$	$1.2 \pm 1.6 \times 10^{6}$	4.9
• All intervals open (A)	4.1×10^{-14}	8.8×10^{-2}	1.2	4.5
• All intervals open (A,B,C,R)	$3.9 \times 10^{-14} \pm 1.6 \times 10^{-15}$	$9.6 \times 10^{-2} \pm 7.0 \times 10^{-3}$	$1.3 \pm 2.2 \times 10^{-2}$	4.5

Table 10
Eigenanalysis of Covariance Matrix of Estimation Errors Obtained from Interpretation of All Injection Steps and Recovery During Test JHB0612

Parameters	Eigenvectors		
k [m^2]	1.000	9.6439×10^{-15}	-7.5978×10^{-16}
ϕ [m^3/m^3]	9.6247×10^{-15}	–0.9998	-2.2232×10^{-2}
ϕ_w [m^3/m^3]	9.7400×10^{-16}	-2.2232×10^{-2}	0.9998
Eigenvalues	6.3155×10^{-31}	6.1682×10^{-6}	1.1690×10^{-2}

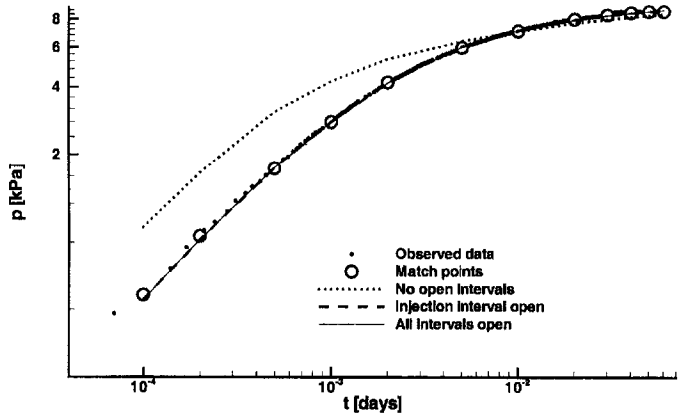

Figure 15. Pressure data from first injection step during test JJA0616 interpreted by various inverse models.

the initial air pressure and, therefore, changes in borehole storage due to air compressibility are minor.

A joint analysis of pressure data from all steps of the test, including recovery, gives a good match (Figure 14) and reasonable estimates (Table 9). As implied by the eigenvectors in Table 10, the model is now sensitive to all three parameters, whose estimates seem reasonable and certain.

Test JJA0616

Results for test JJA0616 are listed in Table 11. Type-curves using spherical and radial flow models (Illman et al. 1998; Illman and Neuman 2000) identified k values which are close to that obtained from steady-state analysis (Guzman et al. 1996). Though the type-curve fits were poor, the radial-flow analysis gave reasonable values for ϕ and C_D (Illman et al. 1998). Numerical inverse

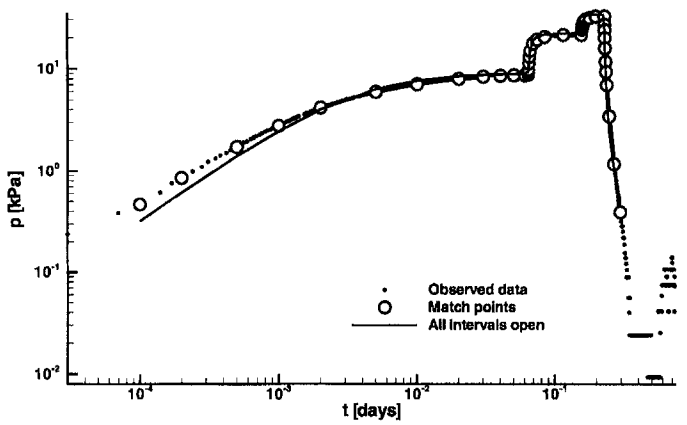

Figure 16. Pressure data from all injection steps and recovery during test JJA0616 interpreted by inverse model.

results are compared with measured values in Figure 15. Again the fit improves greatly when we include the injection interval, leading to more reliable estimates. The fit is equally good and the estimates are similar when we incorporate all open borehole intervals. This is important because among all the tests we have analyzed, this one is the most likely to be influenced by surrounding open boreholes. Borehole V3, only about 2 m from the injection interval (Figure 1), is open to the atmosphere.

The numerical inverse model produced estimates with small errors for all three parameters, based solely on data from the first injection step. This is confirmed by an eigenanalysis of the corresponding covariance matrix (Table 12). As in to test JGC0609, the pressure buildups are comparable to the initial air pressure, and therefore, changes in borehole storage due to changes in air compressibility are substantial. This may explain why type-curve matches were relatively poor in this case (Illman et al. 1998). Still, borehole storage dominates pressure transients and makes it difficult to obtain reasonable estimates of ϕ and ϕ_w; our estimate of ϕ is much too high for fractures (Table 11).

Fitting the inverse model to data from all steps of the test, including its recovery stage, leads to a good overall fit (Figure 16). An eigenanalysis of the covariance matrix demonstrates reliable estimation of all parameters (Table 13). The estimated ϕ value is now much lower and can be considered as representative of fracture properties.

Table 11
Parameter Estimates for Test JJA0616

Type of Analysis	k [m^2]	ϕ [m^3/m^3]	ϕ_w [m^3/m^3]	C_D [–]
Analytical steady-state (A)	5.6×10^{-15}			
Analytical transient				
• Spherical flow (A)	8.0×10^{-15}			
• Radial flow (A)	7.1×10^{-15}	3.1×10^{-2}		1.0×10^{1}
Inverse modeling				
• No open intervals (A)	$5.4 \times 10^{-15} \pm 7.9 \times 10^{-16}$	$5.0 \times 10^{-1} \pm 3.9 \times 10^{-2}$		
• Open injection interval (A)	$4.0 \times 10^{-15} \pm 7.8 \times 10^{-17}$	$1.3 \times 10^{-1} \pm 5.8 \times 10^{-3}$	$1.1 \pm 5.2 \times 10^{-2}$	2.8
• All intervals open (A)	$4.1 \times 10^{-15} \pm 7.1 \times 10^{-17}$	$1.3 \times 10^{-1} \pm 6.4 \times 10^{-3}$	$1.1 \pm 3.9 \times 10^{-2}$	2.8
• All intervals open (A,B,C,R)	$4.3 \times 10^{-15} \pm 1.9 \times 10^{-16}$	$1.8 \times 10^{-2} \pm 3.9 \times 10^{-4}$	$1.6 \pm 72 \times 10^{-2}$	3.0×10^{1}

Table 12
Eigenanalysis of Covariance Matrix of Estimation Errors Obtained from Interpretation of First Step During Test JJA0616

Parameters	Eigenvectors		
k [m^2]	1.000	3.5628×10^{-15}	-1.8002×10^{-16}
ϕ [m^3/m^3]	3.5461×10^{-15}	–0.9983	-5.8609×10^{-2}
ϕ_w [m^3/m^3]	3.8852×10^{-16}	-5.8609×10^{-2}	0.9983
Eigenvalues	8.9518×10^{-34}	7.0241×10^{-6}	2.9162×10^{-4}

Table 13
Eigenanalysis of Covariance of Estimation Errors Obtained from Interpretation of All Injection Steps and Recovery During Test JJA0616

Parameters	Eigenvectors		
k [m^2]	1.000	3.5963×10^{-13}	-4.4528×10^{-16}
ϕ [m^3/m^3]	3.5963×10^{-13}	–1.000	-6.9652×10^{-4}
ϕ_w [m^3/m^3]	1.9479×10^{-16}	-6.9652×10^{-2}	1.00
Eigenvalues	3.5004×10^{-33}	3.6030×10^{-8}	1.2518×10^{-3}

Conclusions

Multirate injection and recovery data from single-hole pneumatic tests in unsaturated fractured tuff at the ALRS are amenable to analysis by means of a three-dimensional numerical inverse model, which considers only isothermal single-phase airflow and treats the rock as a uniform, isotropic equivalent continuum representative of interconnected fractures. Borehole storage depends on air compressibility in the injection interval and decreases with an increase in absolute air pressure. Borehole storage influences pressure transients during the first step of each test and makes it difficult to obtain reliable estimates of air-filled porosity and dimensionless borehole storage coefficient from such data. Pressure transients during subsequent injection steps are affected by borehole storage to a lesser degree than are those during the first step. Recovery data are theoretically free of borehole storage effects. A consideration of the effect of air compressibility on storage and a joint analysis of pressure data from all stages of a single-hole pneumatic test are, therefore, essential for the reliable estimation of air-filled porosity and borehole storage coefficient. The storage effect observed during single-hole tests seems related not only to the injection interval, but also to openings in the surrounding rock. Since open borehole intervals surrounding the injection intervals are relatively far from each other, they have little impact on the measured pressure responses. Air permeabilities obtained by our inverse method are comparable to those obtained by means of steady-state formulae (Guzman et al. 1996) and transient type-curve analyses (Illman et al. 1998); however, the steady-state estimates are slightly lower than those obtained by numerical inverse model from transient data. Except for one of the four cases presented here, analytical transient type-curves (Illman et al. 1998; Illman and Neuman 2000) did not match observed pressure records and did not allow reliable identification of air-filled porosity and borehole storage coefficient. This is due to linearization of the airflow equations. Information about the spatial variability of permeabilites from single-hole pneumatic tests at the ALRS, and their relationship to cross-hole test results, can be found in Chen et al. (2000), Illman and Neuman (2001), and Vesselinov et al. (2001a, 2001b).

Acknowledgments

This research was supported by the United States Nuclear Regulatory Commission under contracts NRC-04-95-038 and NRC-04-97-056. Part of the simulation and inverse modeling was conducted during a summer internship of Velimir V. Vesselinov with the Geoanalysis Group at Los Alamos National Laboratory. We are grateful to George A. Zyvoloski for his help in the implementation of FEHM, and to Carl W. Gable for his assistance in the use of X3D.

References

Bear, J. 1972. *Dynamics of Fluids in Porous Media*. New York: Elsevier.

Benito, P.H., P. Cook, B. Faybishenko, B. Freifeld, and C. Doughty. 1998. Box canyon pneumatic conductivity study: Preliminary data analysis. *Tech Rep. 42359*. Berkeley, California: Lawrence Berkeley National Laboratory.

Benito, P.H., P. Cook, B. Faybishenko, B. Freifeld, and C. Doughty. 1999. Cross-well air-injection packer tests for assessment of pneumatic connectivity in fractured basalt. In *Proceedings of the 37th U.S. Rock Mechanics Symposium*, Vail, Colorado, ed. B. Amadei, R.L. Kranz, G.A. Scott, and P.H. Smealie, 843–850. Rotterdam: A.A. Balkema.

Cardenas, M., C. LeCompte, and G. Cua. 1999. Estimation of permeability of disturbed halite using inverse modeling. *Ground Water* 37, no. 1: 539–545.

Chen, G., W.A. Illman, D.L. Thompson, V.V. Vesselinov, and S.P. Neuman. 2000. Geostatistical, type-curve and inverse analyses of pneumatic injection tests in unsaturated fractured tuffs at the Apache Leap Research Site near Superior, Arizona. In *Dynamics of Fluids in Fractured Rocks,* ed. B. Faybishenko, P.A. Witherspoon, and S.M. Benson. AGU Monograph Series 122, 73–98. Washington, D.C.: American Geophysical Union.

Cherry, T.A., C.W. Gable, and H. Trease. 1996. Three-dimensional wells and tunnels for finite element grids. In *Proceedings of the 5th International Conference on Numerical Grid Generation in Computational Fluid Dynamics and Related Fields*, ed. B.K. Soni, J.F. Thompson, H. Hausser, and P.R. Eiseman. Jackson, Mississippi: Mississippi State University Press.

Cronk, T., J.J. Dexter, R.J. Zinkl, and P.M. Kearl. 1990. Air permeability measurements of the unsaturated Bandelier tuff near Los Alamos, New Mexico. *Journal of Hydrology* 117, 225–240.

Doherty, J. 1997. *Parallel PEST.* Brisbane, Australia: Watermark Computing.

Doherty, J., L. Brebber, and P. Whyte. 1994. *PEST: Model Independent Parameter Estimation.* Brisbane, Australia: Watermark Computing.

Finsterle, S., and B. Faybishenko. 1999. Inverse modeling of a radial multistep outflow experiment for determining unsaturated hydraulic properties. *Advances in Water Resources* 22, no. 5: 431–444.

Finsterle, S., and P. Persoff. 1997. Determining permeability of tight rock samples using inverse modeling. *Water Resources Research* 31, no. 8: 1803–1811.

Finsterle, S., and K. Pruess. 1995. Solving the estimation-identification problem in two-phase flow modeling. *Water Resources Research* 31, no. 4: 913–924.

Guzman, A.G., and S.P. Neuman. 1996. Field air injection experiments. In *Apache Leap Tuff Interval Experiments*, ed. T.C. Rasmussen, S.C. Rhodes, A.G. Guzman, and S.P. Neuman, NUREG/CR-6096, 52–94. Washington, D.C.: U.S. Nuclear Regulatory Commission.

Guzman, A.G., S.P. Neuman, C.F. Lohrstorfer, and R.L. Bassett. 1994. Field hydraulic, pneumatic and tracer tests: Phase I. In *Validation Studies for Assessing Unsaturated Flow and Transport Through Fractured Rock*, ed. R.L. Bassett, S.P. Neuman, T. C. Rasmussen, A.G. Guzman, G.R. Davidson, and C.F. Lohrstorfer, NUREG/CR-6203. Washington, D.C.: U.S. Nuclear Regulatory Commission.

Guzman, A.G., A.M. Geddis, M.J. Henrich, C.F. Lohrstorfer, and S.P. Neuman. 1996. Summary of air permeability data from single-hole injection test in unsaturated fractured tuff at the Apache Leap Research Site: Results of steady-state test interpretation. NUREG/CR-6360. Washington, D.C.: U.S. Nuclear Regulatory Commission.

Huang, K., Y.W. Tsang, and G.S. Bodvarsson. 1999. Simultaneous inversion of air injection tests in fractured unsaturated tuff at Yucca Mountain. *Water Resources Research* 35, no. 8: 2375–2386.

Hvilshoj, S., K.H. Jensen, H.C. Barlebo, and B. Madsen. 1999. Analysis of pumping tests of partially penetrating wells in an unconfined aquifer using inverse numerical optimization. *Hydrogeology Journal* 7, no. 4: 365–379.

Illman, W.A. 1999. Single- and cross-hold pneumatic injection tests in unsaturated fractured tuffs at the Apache Leap Research Site near Superior, Arizona. Ph.D. thesis, Department of Hydrology and Water Resources, University of Arizona, Tucson.

Illman, W.A., and S.P. Neuman. 2000. Type-curve interpretation of multirate single-hole pneumatic injection tests in unsaturated fractured rock. *Ground Water* 38, no. 1: 899–911.

Illman, W.A., and S.P. Neuman. 2001. Type-curve interpretation of a cross-hole pneumatic injection test in unsaturated fractured tuff. *Water Resources Research* 37, 583–604.

Illman, W.A., D.L. Thompson, V.V. Vesselinov, G. Chen, and S.P. Neuman. 1998. Single-and cross-hold pneumatic tests in unsaturated fractured tuffs at the Apache Leap Research Site: Phenomenology, spatial variability, connectivity and scale, NUREG/CR-5559. Washington, D.C.: U.S. Nuclear Regulatory Commission.

Lebbe, L., and W. de Breuck. 1995. Validation of an inverse numerical model for interpretation of pumping tests and a study of factors influencing accuracy of results. *Journal of Hydrology* 172, 61–85.

Lebbe, L., and W. de Breuck. 1997. Analysis of a pumping test in an anisotropic aquifer by use of an inverse numerical model. *Hydrogeology Journal* 5, no. 3: 44–59.

Lebbe, L., and N. van Meir. 2000. Hydraulic conductivity of low permeability sediments inferred from triple pumping test and observed vertical gradients. *Ground Water* 38, no. 1: 76–88.

Lebbe, L., M. Mahauden, and W. de Breuck. 1992. Execution of triple pumping test and interpretation by an inverse numerical model. *Hydrogeology Journal* 1, no. 4: 120–134.

LeCain, G. D. 1996. Air-injection in vertical boreholes in welded and nonwelded tuff, Yucca Mountain, Nevada. USGS Water Resources Investigation Report 96-4262.

LeCain, G.D. 1998. Results from air-injection and tracer testing in the Upper Tiva canyon Bow Ridge fault and Upper Paintbrush contact alcoves of the Exploratory Studies Facility, August 1994 through July 1996. USGS Water Resources Investigation Report 98-4058.

Rasmussen, T.C., D.D. Evans, P.J. Sheets, and J.H. Blanford. 1990. Unsaturated fracture rock characterization methods and data sets at the Apache Leap Tuff Site, NUREG/CR-5596. Washington, D.C.: U.S. Nuclear Regulatory Commission.

Sauer, R., R. Greswell, A. Herbert, R. Mackey, and J. Tellam. 2000. Model calibration from pump testing of the 3D flow around a test well site, penetrating the Triassic Sandstone Aquifer, Birmingham, U.K. In *ModelCare '99 Calibration and Reliability in Groundwater Modelling: Coping with Uncertainty*, ed. F. Stauffer, W. Kinzelbach, K. Kovar, and E. Hoehn. Wallingford, Oxfordshire, U.K.: IAHS.

Trease, H.E., D. George, C.W. Gable, J. Fowler, A. Kuprat, and A. Khamyaseh. 1996. The X3D grid generation system. In *Proceedings of 5th International Conference on Numerical Grid Generation in Computational Fluid Dynamics and Related Fields*, ed. B.K. Soni, J.F. Thompson, H. Hausser, and P.R. Eisenman. Jackson, Mississippi: Mississippi State University Press.

Vesselinov, V.V. 2000. Numerical inverse interpretation of pneumatic tests in unsaturated fractured tuffs at the Apache Leap Research Site. Ph.D. thesis, Department of Hydrology and Water Resources, University of Arizona, Tucson.

Vesselinov, V.V., S.P. Neuman, and W.A. Illman. In press. Three-dimensional numerical inversion of pneumatic cross-hole tests in unsaturated fractured tuff: 1. Methodology and borehole effects. *Water Resources Research.*

Vesselinov, V.V., S.P. Neuman, and W. A. Illman. In press. Three-dimensional numerical inversion of pneumatic cross-hold tests in unsaturated fractured tuff: 2. Equivalent parameters, high-resolution stochastic imaging and scale effects. *Water Resources Research.*

Wang, J.S.Y., P.J. Cook, and R.C. Trautz. 1998. Field testing and observation of flow paths in niches: Phase 1 status report of the drift seepage test and niche moisture study. Technical Report Level 4 Milestone SPC314M4, Yucca Mountain Characterization Project.

Zyvoloski, G.A., and B.A. Robinson. 1995. Models and methods summary for the GZSOLVE application. Technical Report LA-12062-MS Rev. 1. Los Alamos, New Mexico: Los Alamos National Laboratory.

Zyvoloski, G.A., Z.V. Dash, and S. Kelkar. 1988. FEHM: Finite element heat and mass transfer. Technical Report LA-11224-MS. Los Alamos, New Mexico: Los Alamos National Laboratory.

Zyvolski, G.A., B.A. Robinson, Z.V. Dash, and L.L. Trease. 1996. Users manual for the FEHMN application. Technical Report LA-UR-94-3788. Los Alamos, New Mexico: Los Alamos National Laboratory.

Zyvoloski, G.A., B.A. Robinson, Z.V. Dash, and L.L. Trease. 1997. Summary of the models and methods for the FEHM application—A finite-element heat- and mass-transfer code. Technical Report LA-13307-MS. Los Alamos, New Mexico: Los Alamos National Laboratory.